https://doi.org/10.5194/cp-2021-55
Preprint. Discussion started: 3 June 2021

Climate of the Past
Discussions

Different facets of dryness/wetness pattern in southwestern China over the past 27,000 years

Mengna Liao[1 #], **Kai Li**[1 #], **Weiwei Sun**[2], **Jian Ni**[1]

[1] College of Chemistry and Life Sciences, Zhejiang Normal University, Jinhua, 321004, PR China

[2] State Key Laboratory of Lake Science and Environment, Nanjing Institute of Geography and Limnology, Chinese Academy of Sciences, Nanjing, 210008, PR China

Correspondence to: Jian Ni (nijian@zjnu.edu.cn)

Contributing equally.

https://doi.org/10.5194/cp-2021-55
Preprint. Discussion started: 3 June 2021

Climate of the Past
Discussions

Abstract. Frequently happened meta-droughts have arisen broad social attention under current global climate change. A paleoclimatic perspective is expected to gain our understanding on the causes and manifestation more comprehensively. Southwestern China has been threatened by severe seasonal droughts. Our current knowledge of millennial-scale drying/wetting processes in this region is primarily based on the variability of the Indian Summer Monsoon. However, water availability over land does not always follow the monsoonal precipitation but also depends on water loss from evaporation and transpiration. Here, we reconstructed precipitation intensity, lake hydrological balance and soil water stress index (SWSI) covering the last 27,000 yr, based on grain size, geochemical and pollen records from Yilong Lake, to discuss the long-term nexus and discrepancies of dryness/wetness patterns in meteorological, hydrological and soil systems in central Yunnan region, SW China. Our results show that the long-term change trajectories among precipitation, hydrological balance and soil moisture were not completely consistent. During periods of low precipitation, hydrological balance and soil moisture were primarily controlled by temperature-induced evaporation change. This caused opposite status of precipitation with hydrological balance and soil moisture during the Last Glacial Maximum and Younger Dryas. During periods of high precipitation — the early to late Holocene, intensified evaporation from the lake surface offset the effects of increased precipitation on hydrological balance. But meanwhile, abundant rainfall and dense vegetation canopy avoided soil moisture deficit that might result from rising temperature. To sum up, hydrological balance in central Yunnan region was more vulnerable to temperature change while soil moisture could be further regulated by vegetation changes on millennial scale. As such, under future climate warming, surface water shortage in central Yunnan region can be even more serious. But for soil systems, efforts to reforestation may bring some relief to soil moisture deficit in this region.

https://doi.org/10.5194/cp-2021-55
Preprint. Discussion started: 3 June 2021

Climate of the Past
Discussions

1. Introduction

The global land area in extreme-to-exceptional terrestrial water storage drought could more than double by the late twenty-first century (Pokhrel et al., 2021). In southwestern (SW) China, drought has become a climate threat and is likely to happen more frequently in the future (Qiu, 2010; Wang et al., 2016). It is generally deemed that long-term drying/wetting processes in SW China is primarily regulated by the intensity of monsoonal precipitation associated with the evolution of atmospheric circulation systems (Chen et al., 2014; Hillman et al., 2017; Sun et al., 2019; Wang et al., 2019). However, drought relates fundamentally to the amount of water available in soil or hydrological systems, which is obviously depending a lot on precipitation but also on how much water infiltrates to deeper ground layers or runs off the land and how much is evaporated directly from water and soil surfaces or transpired by plants (Breshears et al., 2005; Dai et al., 2018; Feng and Liu, 2015; Mishra and Singh, 2010; Trenberth et al., 2014). Therefore, drought is not necessary to happen during periods of low precipitation, and vice versa (Dai et al., 2018; Sun et al., 2017; Trenberth et al., 2014; Xu et al., 2019). Given this, understanding dryness/wetness patterns in different climate scenarios with considering physical and plant processes is crucial to predicting future drying or moistening.

Climate evolution in SW China since the Last Glacial Maximum (LGM) has been reconstructed using various types of paleoclimatic archives, such as speleothem oxygen isotope records (e.g., Cai et al., 2015; Dykoski et al., 2005; Zhao et al., 2015), lake sediments (e.g., Hillman et al., 2017; Hillman et al., 2020; Hodell et al., 1999; Li et al., 2018; Sun et al., 2019; Wang et al., 2020; Wu et al., 2018; Xiao et al., 2014a; Xiao et al., 2014b; Zhang et al., 2017; Zhang et al., 2019a), and peats (e.g., Huang et al., 2016; Wei et al., 2012). The major viewpoint of these researches is that the monsoonal precipitation was very low during the LGM and peaked in the early Holocene and decreased after that, while the coldest climate appeared in the LGM and the warmest climate in the early to mid-Holocene and a cooling trend followed. The “cold-dry” and “warm-humid” paradigms of climate change in SW China have been widely demonstrated from paleoclimatological perspective, despite a decoupled summer temperature and monsoon precipitation in the early Holocene was proposed (Wu et al., 2018). Additionally, vegetation in SW China had experienced noticeable changes since the LGM (Chen et al., 2014; Cook et al., 2011; Wu et al., 2018; Xiao et al.,

https://doi.org/10.5194/cp-2021-55
Preprint. Discussion started: 3 June 2021

2014a; Xiao et al., 2014b), which may have exerted some influence on evapotranspiration process. Since water availability is a trade-off among precipitation input and water loss through evaporation, transpiration and outflow (Breshears et al., 2005; Dai et al., 2018; Watras et al., 2014), these processes may lead to different conclusions about the wetting or drying patterns over land. But to date, rare studies have tested this idea.

Definitions of "drying" in meteorology, hydrology and biology are different but connected (Mishra and Singh, 2010). In paleoclimatology, drying or moistening processes can be reconstructed by different types of proxies, but the concepts behind are not necessarily the same. For example, grain-size records from several lakes in SW China reflected variations of the Indian Summer Monsoon (ISM) precipitation (Ning et al., 2017; Peng et al., 2019; Sheng et al., 2015). Authigenic carbonate precipitation is strongly affected by hydrological balance or precipitation/evaporation ratio (Leng and Marshall, 2004; Ohlendorf et al., 2013), and thus indicates hydrological dryness/wetness conditions in lake-catchment systems. For terrestrial ecosystems, soil water is the main and direct source of water for most plants and a primary constrain for vegetation composition and biomass. Consequently, soil moisture can theoretically revealed from pollen records. As yet, soil moisture status has been rarely reconstructed based on pollen data, and the similarities and differences among the dryness/wetness patterns revealed from different paleoproxies are seldom discussed.

The Yunnan region is located in the southwestern China (Fig. 1). It is primarily influenced by warm and humid airflow from the Bay of Bengal in summer. Several paleolimnological studies had proved that, since the LGM or the Holocene, precipitation, hydrological condition and vegetation in the Yunnan region had experienced noticeable changes (Hillman et al., 2017; Hillman et al., 2020; Hodell et al., 1999; Ning et al., 2017; Sun et al., 2019; Wu et al., 2018; Xiao et al., 2014a). Whereas, rare of them had applied a multi-proxies approach at the same time scale to explore different aspects of the long-term dryness/wetness patterns. Here we developed the first record of soil water stress index (SWSI) based on a pollen record from Yilong Lake in the Yunnan region to reveal soil moisture change over the past 27,000 years. By comparing the SWSI reconstruction with monsoonal precipitation and hydrological balance revealed from the same core, we aim to discuss the long-term nexus and discrepancies of dryness/wetness patterns in meteorological, hydrological and soil systems in SW China.

https://doi.org/10.5194/cp-2021-55
Preprint. Discussion started: 3 June 2021

2. Materials and methods

2.1 Study site and modern climate

Yilong Lake (23.63–23.70° N, 102.50–102.65° E, 1414 m a.s.l.) is a faulted lake in central Yunnan region, SW China (Fig. 1a). It covers an area of 38 km^2 and has a catchment area of 303.6 km^2 (Wang and Dou, 1998). The average water depth is 2.8 m and the maximum is 6.2 m (Wang and Dou, 1998). Yilong Lake is a freshwater lake and fed by overland runoff, lake surface precipitation and groundwater. All the inflow rivers, except the Chenghe River at the northwest of the Lake, are seasonal rivers (Fig. 1b). There was an only outlet located at the southeast end of the lake when the lake was in highstand, but it disappeared in 1978 CE due to climate- and human-induced lake level dropping (Wang and Dou, 1998).

This region is dominated by subtropical monsoon climate. Observations from the closest meteorological station in the Yuxi City (24.2° N, 102.338° E, 1717 m a.s.l.), 80 km away from Yilong Lake, yield a mean annual temperature of 18.1°C after lapse rate correction (0.65 °C per 100 m) and mean annual precipitation of 886 mm (1951–2017 CE; China Meteorological Data Service Centre, https://data.cma.cn/en). Annual evaporation (1035 mm) in this region is slightly higher than the annual precipitation. The seasonal climate change is characterized by high precipitation in warm season while low precipitation in cold season (Fig. 1c).

2.2 Sampling and dating

In May 2017, a sediment core (YLH) was retrieved from Yilong Lake at a water depth of 4.1 m (Fig. 1b) using a UWITEC sampling system. The sediment core was transported to the laboratory of School of Geography, Nanjing Normal University and kept at 3.9°C until analysis. The sediment core was split with Geotek Core Splitter, photographed and visually described in the laboratory. The samples were separated at 1-cm intervals, freeze-dried, and used for further analyses.

The age of the entire Core YLH was determined using fifteen accelerator mass spectrometry (AMS) ^{14}C dates including bulk organic matter, charcoal and plant remains (Table 1). The measurements were made by Beta Analytic Testing Laboratory. The conventional ^{14}C dates were calibrated using Calib 8.20 with an IntCal20 calibration dataset (Reimer et al., 2020).

https://doi.org/10.5194/cp-2021-55
Preprint. Discussion started: 3 June 2021

Age-depth modelling was performed in R (version 3.4.4, R Core Team, 2018) using the package “rbacon” (Blaauw et al., 2020). According to the age-depth model, the basal sediment was deposited between 27.171–26.439 cal. ka BP with a median age of 27.000 cal. ka BP (Fig. 2).

2.3 Analytical methods

Samples for grain size analysis were determined at 1-cm intervals. All the samples were pretreated by using 30 % H_2O_2 and 5 % HCl to remove organic matter and carbonate, rinsing with deionized water to make the liquid close to neutral, and adding 10 % $(NaPO_3)_6$ to disperse particles on an ultrasonic treatment before grain-size measurement. The grain size distribution was measured by a Malvern 3000E laser diffraction instrument with 100 bins ranging from 0.02 to 2000 μm.

The sediments (collected at 1-cm intervals) were pretreated with 10 % HCl to remove carbonates and then used to measure the total organic carbon (TOC) and total nitrogen (TN) using a vario EL cube Elemental Analyzer. Replicate analyses of well-mixed samples showed that the precision was ca.± <0.1 % (1 standard deviation (s.d.)). Continuous down-core X-ray fluorescence (XRF) measurements of the geochemical composition were carried out with a core scanner (MSCL-S Specifications; tube voltage 15 kV, exposure time 30 s and spatial distribution 0.5) at the laboratory of the School of Geography, Nanjing Normal University. The sample moved along a monochromatized and polarized SR beam. Core scanning started from the depth 10 cm because the upper 10-cm sediments with high water content are too soft to get robust measurements. Core bulk mineralogy of freeze-dried and milled samples (at 2-cm intervals) were derived by X-ray diffraction (XRD) technique using a PANalytical X’pert Pro (40 kV, 30 mA, from 5 to 80°, step-rate 0.0167°, Cu kα radiation) at the Qinghai Institute of Salt Lakes, Chinese Academy of Science (CAS). Seventy one freeze-dried samples from depths where carbonate content is (relatively) high (10–176 cm and 228–280 cm) were measured for oxygen stable isotope in carbonate ($^{18}O_{carb}$) using a Thermo-Fisher MAT 253 mass spectrometer equipped with a Kiel-IV carbonate preparation device at the Nanjing Institute of Geography and Limnology, CAS. The samples were pretreated with 100% phosphoric acid. The $^{18}O_{carb}$ values are expressed as standard delta (δ) notation as the per mil (‰) deviation from Vienna Pee Dee Belemnite (VPDB). Four samples at different depths were imaged using a Hitachi

https://doi.org/10.5194/cp-2021-55
Preprint. Discussion started: 3 June 2021

SU8010 scanning electron microscope (SEM) to examine crystal structure and morphology of carbonate minerals.

Samples for pollen analysis were determined at 4-cm intervals and treated using standard laboratory methods (Faegri et al., 1989), including treatment with 10 % HCl and 50 % HF to remove carbonate and silicate, boiling in 10 % KOH to remove humic acid, sieving to remove the fine and coarse fractions, and mounting in silicone oil. To calculate the concentrations of pollen, tablets containing a known quantity of *Lycopodium* spores were added to each sample prior to the treatments. At least 300 terrestrial pollen grains per sample were counted. All the treatment and identification works were processed in the Institute of Hydrogeology and Environmental Geology, Chinese Academy of Geological Sciences. The pollen percentages were calculated based on the total number of pollen grains from terrestrial pollen taxa and used to construct a pollen diagram and conduct numerical analyses.

2.4 Pollen-based quantitative reconstruction of SWSI

In total, 1394 surface soil pollen samples from SW China (Ni et al., 2014; Fig. S1 in the Supplement) are employed in this study. Annual climate data was averaged from long-term records from 1971 to 2000 at 1814 meteorological stations across China (China Meteorological Data Service Centre, https://data.cma.cn/en). These data was interpolated into 1 km grid cells using a thin plate smoothing spline surface fitting technique (Hancock and Hutchinson, 2006) that takes the impact of elevation into account on the basis of the SRTM digital elevation model (Farr et al., 2007). The interpolation was performed in the program ANUSPLIN version 4.36 (Hutchinson, 2006). The interpolated meteorological data were used to calculate the SWSI on the basis of the SPLASH v.1.0 (Davis et al., 2017). SWSI reflects the degree of evapotranspiration deficit and is expressed as (PET-AET)/PET, where AET and PET are the annual sums of actual and potential evapotranspiration, respectively (Prentice et al., 1993). The SWSI reconstruction was made using the weighted-averaging partial least square (WA-PLS) regression (ter Braak and Juggins, 1993). The pollen percentages were square-root transformed to stabilize variances and optimize the signal-to-noise ratio (Prentice, 1980). The 'leave-one-out' cross-validation was used to test the reliability and robustness of the model. The number of components to include in the transfer function was selected as those producing the lowest

https://doi.org/10.5194/cp-2021-55
Preprint. Discussion started: 3 June 2021

root mean squared error of prediction (*RMSEP*), a high coefficient of determination between observed and predicted environmental values (r^2) and low average bias(ter Braak and Juggins, 1993). These analyses were carried out using R package "rioja" (Juggins, 2017).

3. Results

3.1 Grain size and geochemical data of core YLH

Grain size in core YLH are mainly composed of clay (< 4 μm) and silt (4–63 μm), with mean contributions of 25 % and 70.2 %, respectively. Down-core variations of clay component exhibit generally high values during ca. 16–27.5 cal. ka BP (ca. 246–456 cm) and ca. 0–3 cal. ka BP (ca. 0–40 cm), and low values with strong fluctuations during ca. 3–16 cal. ka BP (ca. 41–245 cm) (Fig. 3). The variations of silt component are basically contrary to that of clay component. The sand component is characterized by low percentages throughout the core (average percentage of 4.8 %) and punctuated by two intervals (ca. 3–5 cal. ka BP and ca. 13–16 cal. ka BP) with slight increase in the percentages (average ca. 8–10 %) (Fig. 3). The median size was small during ca. 15–27.5 cal. ka BP (ca. 235–456 cm) and ca. 0–2 cal. ka BP (ca. 0–26 cm). In the period of 2–15 cal. ka BP, the median size was relatively big but around 11 cal. ka BP, it is as small as that in other periods (Fig. 3).

TOC within the samples differs between 0.75 % and 15.13 %, and TN varies from 0.08% to 2.01 % (Fig. 3). TOC increases from 9 % to 15 % during 27.5–20 cal. ka BP then decreases to 5 % around 12–9 cal. ka BP; it followed by a sudden increase to 10–14 % after that and then a sharp decrease to 0.75 % during 5–3 cal. ka BP and increases again since then (Fig. 3). Variations of TN is highly synchronous with that of TOC (Fig. 3). The C/N ratio is about 10 during 27.5–13 cal. ka BP and larger than 10 during 8–7 and 5–3 cal. ka BP while smaller than 10 during 13–8, 7–5 and 3–0 cal. ka BP (Fig. 3). The Fe/Mn ratio illustrates a remarkable high value around 13–9 cal. ka BP (Fig. 3).

XRD detects quartz, calcite, aragonite, magnetite, muscovite, gypsum, rhodochrosite, dolomite, clinochlore as major minerals in the core sediments. Carbonate in the core appears primarily in two sections 0–180 cm and 226–288 cm (Fig. 3). Aragonite exists only in the upper 34-cm sediments, which partially compensate the decrease of calcite (Fig. 3). The $\delta^{18}O_{carb}$ value vary from -8.435 to -2.525 ‰during 18 to 14.5 cal. ka BP and from -10.472 to -4.371 ‰ during

https://doi.org/10.5194/cp-2021-55
Preprint. Discussion started: 3 June 2021

Climate of the Past Discussions

8.5–0.77 cal. ka BP (Fig. 3). $^{18}O_{carb}$ enriched consistently since 8.5 cal. ka BP (Fig. 3).

3.2 Variations of pollen assemblages and reconstructed SWSI over the past 27,000 years

A total of 99 pollen types were identified in 114 samples. Pollen of the tree taxa, including primarily *Pinus*, *Picea*, evergreen and deciduous *Quercus* (*Quercus*.Eve and *Quercus*.Dec), *Betula* and *Tsuga*, dominated the entire pollen record, with an average percentage of 85.6 % (Fig. 4). The shrub taxa occupies only 1.08 % of the entire pollen record. Average percentage of the herbaceous taxa is 13.3 %. Among the herb taxa, only *Artemisia*, Poaceae and Asteraceae have average percentages >1%. Herbs increased remarkably in several brief time intervals between 8−6 cal. ka BP and between 3−2 cal. ka BP (Fig. 4). The most noticeable change of tree pollen composition happened around 13 cal. ka BP, for which *Quercus*.Dec was replaced rapidly by *Quercus*.Eve and coniferous tree pollen (*Abies*, *Picea*, *Pinus* and *Tsuga*) almost disappeared (Fig. 4). Another outstanding change of pollen composition occurred at 3 cal. ka BP, for which *Pinus*, *Artemisia* and Poaceae increased considerably, and *Quercus*.Eve, *Quercus*.Dec *Betula* and *Alnus* decreased correspondingly. The average percentage of herbs was relatively low compared with woody plants throughout the core. But the abundance of herbaceous pollen increased noticeably between 8−6 cal. ka BP and especially after 3 cal. ka BP, with the maximum percentage reaching up to more than 90 %.

Two-component WA-PLS model was selected on the basis of high r^2 (0.62), low *RMSEP* (0.159) and the smallest number of 'useful' components (Table S1 in the Supplement). High (low) SWSI value indicates big (small) water stress in soil system. The reconstructed SWSI ranges from 0 to 0.29, reflecting low to moderate water stress over the past 27,000 years. Relatively high SWSI appeared in three periods: 20−15 cal. ka BP, 8−6 cal. ka BP and 4−0 cal. ka BP (Fig. 4).

4. Discussion

4.1 Precipitation change revealed by grain size

Grain size composition in lake sediments contains information on the sources of clastic materials, lake level fluctuations and transport energy related to variations in runoff (Peng et al., 2005; Xiao et al., 2013). Yilong Lake is located in the realm of the ISM, where the source of clastic

https://doi.org/10.5194/cp-2021-55
Preprint. Discussion started: 3 June 2021

materials (especially coarse particles) and the transport energy are primarily controlled by the precipitations. Previous study on the spatial characteristics of grain-size distributions in the surface sediments of Yilong lake revealed that, as the decrease of water depth, the median size increases and the grain-size distribution curve changes from a "unimodal" to "bimodal" shape (Zhang et al., 2019b). In the core YLH, most of the samples with relatively big median grain size show a "unimodal" but not a "bimodal" distribution mode (Fig. S2 in the Supplement), which implies a relatively high lake level and that transport energy was likely to be the main cause for changes in the grain-size components. Consequently, the increased sand component and median grain size coarsening should relate to intensified hydrological energy under increased precipitation.

Carbonate deposited from the lake water was assumed to preserve the $\delta^{18}O$ signal of precipitation and hence the $\delta^{18}O_{carb}$ from lake sediments is a good proxy for reflecting intensities of precipitation or ISM in Yunnan region (Hillman et al., 2017; Hillman et al., 2020; Hodell et al., 1999; Sun et al., 2019). A moderately strong negative correlation between precipitation $\delta^{18}O$ and monthly precipitation amount at Kunming has been reported (Hillman et al., 2017). Conclusion that the $\delta^{18}O$ of the water in Yilong Lake was controlled by the $\delta^{18}O$ of precipitation should be reasonable. The changes of median grain size in core YHL resemble well with that of $\delta^{18}O_{carb}$, with small grain size corresponding to high $\delta^{18}O_{carb}$ value, and vice versa (Fig. 5). This supports that the median grain size is a reliable indicator of precipitation intensity in Yilong Lake. However, it should be noted that grain-size data from the samples of the recent 3,000 years cannot be simply interpreted as changes in precipitation intensity because human activities exerted strong impacts on the regional landscape and water systems during this period (Wu et al., 2015; Xiao et al., 2017).

Variations of the median grain size from core YLH reflect less monsoonal precipitation during ca. 27–15 cal. ka BP and generally high precipitation between ca. 15–3 cal. ka BP (Fig. 5). This pattern is basically consistent with many lines of evidence from stalagmites (Cai et al., 2015; Cheng et al., 2016; Dykoski et al., 2005; Zhao et al., 2015) and lake sediments (Hodell et al., 1999; Peng et al., 2019; Sun et al., 2019). Besides, variations of the median grain size also record the well-known climatic events Bølling/Allerød (B/A) and Younger Dryas (YD), showing respectively as sharp increase and decrease of the monsoonal precipitation (Fig. 4). The occurrence time of B/A event in this study is consistent with that documented in the stalagmite $\delta^{18}O$ records from Cave Dongge (Dykoski et al., 2005), Sanbao (Cheng et al., 2016) and Xiaobailong (Cai et al., 2015) (Fig.

5). However, the YD event in this study lagged ca. 1,000 years behind the event recorded in the stalagmite $\delta^{18}O$ from Cave Dongge (Dykoski et al., 2005) and Sanbao (Cheng et al., 2016). Whereas, this delayed monsoon signal can be tracked in the stalagmite $\delta^{18}O$ record from Cave Xiaobailong (Cai et al., 2015) which is only ca. 85 km away from Yilong Lake. Mechanisms behind such discrepancy is beyond the scope of this study, but we considered uneven rainfall distribution due to the complex topography of the Yunnan-Guizhou Plateau should have played an important role.

4.2 Carbonate deposition as a recorder of past hydrological balance

Carbonate deposition in Yilong Lake mainly comprise autochthonous calcite and aragonite (Fig. S3 in the Supplement), which is similar with two nearby shallow Lakes Xingyun and Qilu. A large amount of mollusk shells are the main source of aragonite that only appear in the upper 34-cm sediments. Autochthonous calcite precipitation need a certain degree of supersaturation (Raidt and Koschel, 1988) which can be achieved by seasonal temperature increase and plankton flourishing (Robbins and Blackwelder, 1992; Stabel, 1986). ^{18}O measurements of the lake water and precipitation indicated significant evaporative effects in Yilong basin during warm season (Whitmore et al., 1997). Increased temperature exerts a direct control on water evaporation, which will concentrate dissolved carbonate and hence facilitate carbonate precipitation. Photosynthesis of plankton influences carbonate precipitation by affecting CO_2 and pH in the epilimnetic water and/or providing nucleation sites for crystallization (Robbins and Blackwelder, 1992; Stabel, 1986). Assuming that lake primary productivity played a big role in carbonate precipitation, algae productivity should have increased during 20–14 cal. ka BP when carbonate content increased, and decreased during 14–9 cal. ka BP when carbonate content decreased. But in fact, relatively high C/N values in 20–14 cal. ka BP and low in 14–9 cal. ka BP indicate relatively low and high algae productivity, respectively. In addition, characteristics of the crystal morphology of calcite also indicate abiotic origins (Fig. S3 in the Supplement). We consequently believe that lake primary productivity is not a main cause for carbonate precipitated in Yilong Lake. Carbonate content in the lake sediments should reflect hydrological balance (i.e. P-E).

According to the variations of carbonate content in the lake sediments (Fig. 3), we considered a relatively positive water balance in 27–20 cal. ka BP and 14–9 cal. ka BP, and a negative water balance in 20–14 cal. ka BP and 9–0 cal. ka BP. In addition, carbonate records from the two

https://doi.org/10.5194/cp-2021-55
Preprint. Discussion started: 3 June 2021

nearby shallow Lakes Xingyun and Qilu (Fig.1, Hillman et al., 2017; Hillman et al., 2020; Hodell et al., 1999) show a broadly similar patterns with our record, indicating that the hydrological changes reconstructed from the present study reflect a regional rather than a local climate signal.

4.3 Different patterns of long-term changes in precipitation, hydrological balance and SWSI, and the potential mechanisms

Precipitation is the primary water supply for lacustrine system and soils. It is traditionally believed a dry condition when precipitation was low, while wet condition when precipitation was high. From this point of view, we may conclude that our study region went through a “dry” condition during the cold LGM and a “wet” condition during the warm Holocene. This pattern is basically in line with other paleoclimate reconstructions in the Yunnan region (e.g., Cheng et al., 2016; Xiao et al., 2014b). However, it does not match well with the reconstructions of hydrological balance and SWSI from the same core. During the LGM (27–20 cal. ka BP) and the YD event, precipitation was low but water balance of the Yilong Lake was positive and the soil moisture was relatively high. During the early to late Holocene (9–3 cal. ka BP), precipitation was high but the water balance was negative. The essence of dryness is the shortage of available water, which is fundamentally a trade-off between water input and output (Breshears et al., 2005; Dai et al., 2018; Mishra and Singh, 2010; Trenberth et al., 2014; Watras et al., 2014). Therefore, factors controlling water loss from terrestrial systems also play a big role in the formation of a dry condition.

Evaporation is one of the important ways of water loss from land. Evaporation rate is higher at higher temperature because as temperature increases, the average kinetic energy of the molecules increases and hence more molecules fly off the surface. The LGM was characterized by low temperature under which the simulated annual-mean potential evapotranspiration decreased by 10–40% over nearly all land (Scheff et al., 2017). In addition, decreased evaporation was a major factor that increases summer effective moisture availability and profoundly influences the hydrological states of lakes (Aichner et al., 2019). These can explain the positive hydrological balance and relatively wet soils during the LGM. Precipitation during 20–15 cal. ka BP was as low as the previous period while insolation was increasing (Fig. 5). This period corresponds to the late glacial warming which had been widely reported from Yunnan region (Fig. 5, Wang et al., 2020; Xiao et al., 2014b; Zhang et al., 2019a). The increased temperature would intensify evaporation and

https://doi.org/10.5194/cp-2021-55
Preprint. Discussion started: 3 June 2021

leading to the water deficiency in lacustrine and soil environments. Therefore, we believed that the hydrological and soil drying during 20–15 cal. ka BP was triggered by the warming temperature. However, in spite of the high temperature, soil moisture was still relatively high during 9–3 cal. ka BP (Fig. 5). Water loss from soil systems is more complex than that from free water surface because, in addition to temperature, underlying surface conditions affect the ways and the amount of soil water loss or soil water storage capacity (Maxwell and Condon, 2016; Zhang and Schilling, 2006).

In a rainfall process, water is redistributed with a big portion of the precipitation intercepted by leaves, stored in soil profile or travelling downhill as surface runoff or infiltrating into to a groundwater body. The amount of water stored in soil profiles and aquifers can be regulated by plant processes (Guzha et al., 2018; Mohammad and Adam, 2010). Previous studies had shown that, no matter at the stand or global scales, plant transpiration accounts for the largest portion of the total evapotranspiration (61 % ± 15 % s.d.–64 % ± 13 % s.d., Good et al., 2015; Maxwell and Condon, 2016; Schlesinger and Jasechko, 2014). Our results show that pollen concentration was high during 9–3 cal. ka BP. Although there is no apparent linear correlations between pollen concentration and vegetation cover (Luo et al., 2009; Xu et al., 2007), changes in the average concentration from late Pleistocene to Holocene by more than three times in a single core can be interpreted as relatively big changes of the plant biomass through time. Increase in aboveground biomass must have increase vegetation canopy and root biomass density (Cairns et al., 1997), causing more water loss from deeper soil layers and aquifers by transpiration through leave stomata rather than loss directly from shallow soil by evaporation (Lawrence and Slingo, 2004; Markewitz et al., 2010). Although high temperature and high plant biomass probably caused increase in the total evapotranspiration during the early to middle Holocene, the abundant precipitation and denser canopy avoided soil moisture deficit that might result from temperature-induced evaporation.

It is seemingly that, over the recent 3,000 years, meteorological, hydrological and soil systems were all in a dry phase (Fig. 5). At the same time, human activities had intensively changed the underlying surface conditions of Yunnan region (Xiao et al., 2017; Xiao et al., 201). *Pinus* sp. are typical pioneer species, which can colonize disturbed sites if competition and grazing pressure are low. Increases in Poaceae pollen abundance is commonly interpreted as increased regional aridity, but also influenced by early farming impact. If climate change was the only critical cause for vegetation change during the recent 3,000 years, vegetation composition should have changed to a status similar to that in the previous “cool-dry” period. However, this probability is disputed as the cluster analysis showing samples from the recent 3,000-year sediments appear in all three clusters representing the late glacial period, the early Holocene and the mid- to late Holocene, respectively (Fig. S4 in the Supplement). Therefore, the pollen-based SWSI probably failed to reflect the real soil moisture condition for the recent 3,000 years. At present, we can hardly estimate how much impact human activities had on lake hydrologic regime and watershed landscape in this period. Thus, the reconstructions of the monsoonal precipitation, hydrological balance and soil moisture for the past 3,000 years are more or less problematic.

5. Conclusions

Sedimentological and pollen data from Yilong Lake provide a 27,000-yr perspective of local or regional variations of ISM precipitation, hydrological balance and soil moisture condition in SW China. The results show that the reconstructed precipitation was basically consistent with the regional pattern, with low precipitation during the LGM and the YD event and high precipitation during the B/A event and the early to middle Holocene. But over the period since the LGM, the long-term change trajectories of precipitation, hydrological balance and soil moisture are not completely consistent. On a millennial scale, hydrological balance was more sensitive to temperature change which controls directly the lake surface evaporation rate. In addition to precipitation and temperature, plant processes may also play a big role in regulating soil moisture. Plant biomass in the Yilong area increased during the early to middle Holocene as documented by the pollen records. This must have increase the vegetation canopy, causing less water loss from shallow soil by evaporation. Human activities became intensive during the recent 3,000 years. It is hardly to estimate how much impact human activities had on the regional landscape and watershed hydrology. Consequently, the deficit in hydrological and soil systems during this period cannot be simply interpreted as climate change. Our study highlights that “wetness” and “dryness” should be precisely defined when interpreting different paleoproxies.

Acknowledgements

This study was supported by the National Basic Research Program of China

(2016YFC0502101), the Strategic Priority Research Program of the Chinese Academy of Sciences (XDA2009000003), the Strategic Priority Research Program of Chinese Academy of Sciences (XDB40000000) and the funding from Nanjing Institute of Geography and Limnology, Chinese Academy of Sciences (2021NIGLAS-CJH03). We appreciated Zhujun Hu, Hongbo Zheng and Yuan Xu from Nanjing Normal University for their help during the XRF core-scanning.

References

Ahn, J., Wahlen, M., Deck, B. L., Brook, E. J., Mayewski, P. A., Taylor, K. C., and White, J. W.: A record of atmospheric CO_2 during the last 40,000 years from the Siple Dome, Antarctica ice core, J. Geophys. Res.-Atmos., 109, D13305, https://doi.org/10.1029/2003JD004415, 2004.

Aichner, B., Makhmudov, Z., Rajabov, I., Zhang, Q., Pausata, F. S., Werner, M., Heinecke, L., Kuessner, M. L., Feakins, S. J., and Sachse, D.: Hydroclimate in the Pamirs was driven by changes in precipitation-evaporation seasonality since the Last Glacial Period, Geophys. Res. Lett., 46, 13972–13983, https://doi.org/10.1029/2019GL085202, 2019.

Blaauw, M., Christen, J. A., and L., M. A. A.: rbacon: Age-depth modelling using Bayesian statistics. R package version 2.5.0. [code], https://CRAN.R-project.org/package=rbacon, 2020.

Breshears, D. D., Cobb, N. S., Rich, P. M., Price, K. P., Allen, C. D., Balice, R. G., Romme, W. H., Kastens, J. H., Floyd, M. L., and Belnap, J.: Regional vegetation die-off in response to global-change-type drought, P. Natl. Acad. Sci. USA, 102, 15144–15148, https://doi.org/10.1073/pnas.0505734102, 2005.

Cai, Y., Fung, I. Y., Edwards, R. L., An, Z., Cheng, H., Lee, J.-E., Tan, L., Shen, C.-C., Wang, X., and Day, J. A.: Variability of stalagmite-inferred Indian monsoon precipitation over the past 252,000 y, . Natl. Acad. Sci. USA, 112, 2954–2959, https://doi.org/10.1073/pnas.1424035112, 2015.

Cairns, M. A., Brown, S., Helmer, E. H., and Baumgardner, G. A.: Root biomass allocation in the world's upland forests, Oecologia, 111, 1–11, https://doi.org/10.1007/s004420050201, 1997.

Chen, X., Chen, F., Zhou, A., Huang, X., Tang, L., Wu, D., Zhang, X., and Yu, J.: Vegetation history, climatic changes and Indian summer monsoon evolution during the Last Glaciation (36,400–13,400 cal yr BP) documented by sediments from Xingyun Lake, Yunnan, China, Palaeogeogr. Palaeocl., 410, 179–189, https://doi.org/10.1016/j.palaeo.2014.05.027, 2014.

Cheng, H., Edwards, R. L., Sinha, A., Spötl, C., Yi, L., Chen, S., Kelly, M., Kathayat, G., Wang, X., and

https://doi.org/10.5194/cp-2021-55
Preprint. Discussion started: 3 June 2021

Li, X.: The Asian monsoon over the past 640,000 years and ice age terminations, Nature, 534, 640–646, https://doi.org/10.1038/nature18591, 2016.

Cook, C. G., Jones, R. T., Langdon, P. G., Leng, M. J., and Zhang, E.: New insights on Late Quaternary Asian palaeomonsoon variability and the timing of the Last Glacial Maximum in southwestern China, Quaternary Sci. Rev., 30, 808–820, https://doi.org/10.1016/j.quascirev.2011.01.003, 2011.

Dai, A., Zhao, T., and Chen, J.: Climate change and drought: A precipitation and evaporation perspective, Curr. Clim. Change Rep., 4, 301–312, https://doi.org/10.1007/s40641-018-0101-6, 2018.

Davis, T., Prentice, I. C., Stocker, B., Thomas, R., Whitley, R., Wang, H., Evans, B., Gallego-Sala, A., Sykes, M., and Cramer, W.: Simple process-led algorithms for simulating habitats (SPLASH v. 1.0): robust indices of radiation, evapotranspiration and plant-available moisture, Geosci. Model Dev., 10, 689–708, https://doi.org/10.5194/gmd-10-689-2017, 2017.

Dykoski, C. A., Edwards, R. L., Cheng, H., Yuan, D., Cai, Y., Zhang, M., Lin, Y., Qing, J., An, Z., and Revenaugh, J.: A high-resolution, absolute-dated Holocene and deglacial Asian monsoon record from Dongge Cave, China, Earth Planet. Sc. Lett., 233, 71–86, https://doi.org/10.1016/j.epsl.2005.01.036, 2005.

Faegri, K., Kaland, P. E., and Krzywinski, K.: Textbook of pollen analysis, John Wiley & Sons Ltd., Chichester, United Kingdom, 1989.

Farr, T. G., Rosen, P. A., Caro, E., Crippen, R., Duren, R., Hensley, S., Kobrick, M., Paller, M., Rodriguez, E., Roth, L., Seal, D., Shaffer, S., Shimada, J., Umland, J., Werner, M., Oskin, M., Burbank, D., and Alsdorf, D.: The shuttle radar topography mission, Rev. Geophys., 45, Art. No. RG2004, https://doi.org/10.1029/2005RG000183, 2007.

Feng, H. and Liu, Y.: Combined effects of precipitation and air temperature on soil moisture in different land covers in a humid basin, J. Hydrol., 531, 1129–1140, https://doi.org/10.1016/j.jhydrol.2015.11.016, 2015.

Good, S. P., Noone, D., and Bowen, G.: Hydrologic connectivity constrains partitioning of global terrestrial water fluxes, Science, 349, 175–177, https://doi.org/10.1126/science.aaa5931, 2015.

Guzha, A., Rufino, M. C., Okoth, S., Jacobs, S., and Nóbrega, R.: Impacts of land use and land cover change on surface runoff, discharge and low flows: Evidence from East Africa, J. Hydrol.-Reg. Stud., 15, 49–67, https://doi.org/10.1016/j.ejrh.2017.11.005, 2018.

Hancock, P. A. and Hutchinson, M.: Spatial interpolation of large climate data sets using bivariate thin plate smoothing splines, Environ. Modell. Softw., 21, 1684–1694, https://doi.org/10.1016/j.envsoft.2005.08.005, 2006.

Hillman, A. L., Abbott, M. B., Finkenbinder, M. S., and Yu, J.: An 8,600 year lacustrine record of summer monsoon variability from Yunnan, China, Quaternary Sci. Rev., 174, 120–132, https://doi.org/10.1016/j.quascirev.2017.09.005, 2017.

Hillman, A. L., O'Quinn, R. F., Abbott, M. B., and Bain, D. J.: A Holocene history of the Indian monsoon from Qilu Lake, southwestern China, Quaternary Sci. Rev., 227, 106051, https://doi.org/10.1016/j.quascirev.2019.106051, 2020.

Hodell, D. A., Brenner, M., Kanfoush, S. L., Curtis, J. H., Stoner, J. S., Xueliang, S., Yuan, W., and Whitmore, T. J.: Paleoclimate of southwestern China for the past 50,000 yr inferred from lake sediment records, Quaternary Res., 52, 369–380, https://doi.org/10.1006/qres.1999.2072, 1999.

Huang, C., Wei, G., Ma, J., and Liu, Y.: Evolution of the Indian summer monsoon during the interval 32.7–11.4 cal. ka BP: Evidence from the Baoxiu peat, Yunnan, southwest China, J. Asian Earth Sci., 131, 72–80, https://doi.org/10.1016/j.jseaes.2016.09.008, 2016.

Hutchinson, M. (Ed.): ANUSPLIN version 4.36 user guide, Centre for Resource and Environmental Studies, the Australian National University, Canberra, Canada, 2006.

Juggins, S.: rioja: Analysis of Quaternary Science Data, R package version (0.9-15.1) [code], http://cran.r-project.org/package=rioja, 2017.

Lawrence, D. M. and Slingo, J. M.: An annual cycle of vegetation in a GCM. Part I: implementation and impact on evaporation, Clim. Dynam., 22, 87–105, http://doi.org/10.1007/s00382-003-0366-9, 2004.

Leng, M. J. and Marshall, J. D.: Palaeoclimate interpretation of stable isotope data from lake sediment archives, Quaternary Sci. Rev., 23, 811–831, https://doi.org/10.1016/j.quascirev.2003.06.012, 2004.

Li, Y., Chen, X., Xiao, X., Zhang, H., Xue, B., Shen, J., and Zhang, E.: Diatom-based inference of Asian monsoon precipitation from a volcanic lake in southwest China for the last 18.5 ka, Quaternary Sci. Rev., 182, 109–120, https://doi.org/10.1016/j.quascirev.2017.11.021, 2018.

Luo, C., Zheng, Z., Tarasov, P., Pan, A., Huang, K., Beaudouin, C., and An, F.: Characteristics of the modern pollen distribution and their relationship to vegetation in the Xinjiang region, northwestern China, Rev. Palaeobot. Palyno., 153, 282–295, https://doi.org/10.1016/j.revpalbo.2008.08.007, 2009.

https://doi.org/10.5194/cp-2021-55
Preprint. Discussion started: 3 June 2021

Markewitz, D., Devine, S., Davidson, E. A., Brando, P., and Nepstad, D. C.: Soil moisture depletion under simulated drought in the Amazon: impacts on deep root uptake, New Phytol., 187, 592–607, https://doi.org/10.1111/j.1469-8137.2010.03391.x, 2010.

Maxwell, R. M. and Condon, L. E.: Connections between groundwater flow and transpiration partitioning, Science, 353, 377–380, http://doi.org/10.1126/science.aaf7891, 2016.

Mishra, A. K. and Singh, V. P.: A review of drought concepts, J. Hydrol., 391, 202–216, https://doi.org/10.1016/j.jhydrol.2010.07.012, 2010.

Mohammad, A. G. and Adam, M. A.: The impact of vegetative cover type on runoff and soil erosion under different land uses, Catena, 81, 97–103, https://doi.org/10.1016/j.catena.2010.01.008, 2010.

Ni, J., Cao, X., Jeltsch, F., and Herzschuh, U.: Biome distribution over the last 22,000 yr in China, Palaeogeogra. Palaeocl., 409, 33–47, https://doi.org/10.1016/j.palaeo.2014.04.023, 2014.

Ning, D., Zhang, E., Sun, W., Chang, J., and Shulmeister, J.: Holocene Indian Summer Monsoon variation inferred from geochemical and grain size records from Lake Ximenglongtan, southwestern China, Palaeogeogra. Palaeocl., 487, 260–269, https://doi.org/10.1016/j.palaeo.2017.09.008, 2017.

Ohlendorf, C., Fey, M., Gebhardt, C., Haberzettl, T., Lücke, A., Mayr, C., Schäbitz, F., Wille, M., and Zolitschka, B.: Mechanisms of lake-level change at Laguna Potrok Aike (Argentina)–insights from hydrological balance calculations, Quaternary Sci. Rev., 71, 27–45, https://doi.org/10.1016/j.quascirev.2012.10.040, 2013.

Peng, J., Yang, X., Toney, J. L., Ruan, J., Li, G., Zhou, Q., Gao, H., Xie, Y., Chen, Q., and Zhang, T.: Indian Summer Monsoon variations and competing influences between hemispheres since ~35 ka recorded in Tengchongqinghai Lake, southwestern China, Palaeogeogra. Palaeocl., 516, 113–125, https://doi.org/10.1016/j.palaeo.2018.11.040, 2019.

Peng, Y., Xiao, J., Nakamura, T., Liu, B., and Inouchi, Y.: Holocene East Asian monsoonal precipitation pattern revealed by grain-size distribution of core sediments of Daihai Lake in Inner Mongolia of north-central China, Earth Planet. Sc. Lett., 233, 467–479, https://doi.org/10.1016/j.epsl.2005.02.022, 2005.

Pokhrel, Y., Felfelani, F., Satoh, Y., Boulange, J., Burek, P., Gädeke, A., Gerten, D., Gosling, S. N., Grillakis, M., and Gudmundsson, L.: Global terrestrial water storage and drought severity under climate change, Nat. Clim. Change, 11, 226–233, https://doi.org/10.1038/s41558-020-00972-w, 2021.

Prentice, I. C.: Multidimensional scaling as a research tool in Quaternary palynology: a review of theory and methods, Rev. Palaeobot. Palyno., 31, 71–104, https://doi.org/10.1016/0034-6667(80)90023-8, 1980.

Prentice, I. C., Sykes, M. T., and Cramer, W.: A simulation model for the transient effects of climate change on forest landscapes, Ecol. Model., 65, 51–70, https://doi.org/10.1016/0304-3800(93)90126-D, 1993.

Qiu, J.: China drought highlights future climate threats: Yunnan's worst drought for many years has been exacerbated by destruction of forest cover and a history of poor water management, Nature, 465, 142–144, http://doi.org/10.1038/465142a, 2010.

R Core Team: R: A language and environment for statistical computing., R Foundation for Statistical Computing [code], https://www.R-project.org/, 2018.

Raidt, H. and Koschel, R.: Morphology of calcite crystals in hardwater lakes, Limnologica, 19, 3–12, 1988.

Reimer, P. J., Austin, W. E. N., Bard, E., Bayliss, A., Blackwell, P. G., Ramsey, C. B., Butzin, M., Cheng, H., Edwards, R. L., Friedrich, M., Grootes, P. M., Guilderson, T. P., Hajdas, I., Heaton, T. J., Hogg, A. G., Hughen, K. A., Kromer, B., Manning, S. W., Muscheler, R., Palmer, J. G., Pearson, C., van der Plicht, J., Reimer, R. W., Richards, D. A., Scott, E. M., Southon, J. R., Turney, C. S. M., Wacker, L., Adolphi, F., Büntgen, U., Capano, M., Fahrni, S. M., Fogtmann-Schulz, A., Friedrich, R., Köhler, P., Kudsk, S., Miyake, F., Olsen, J., Reinig, F., Sakamoto, M., Sookdeo, A., and Talamo, S.: The IntCal20 Northern Hemisphere radiocarbon age calibration curve (0–55 kcal BP), Radiocarbon, 62, 725–757, http://doi.org/10.1017/RDC.2020.41, 2020.

Robbins, L. and Blackwelder, P.: Biochemical and ultrastructural evidence for the origin of whitings: A biologically induced calcium carbonate precipitation mechanism, Geology, 20, 464–468, http://doi.org/10.1130/0091-7613(1992)020<0464:BAUEFT>2.3.CO;2, 1992.

Scheff, J., Seager, R., Liu, H., and Coats, S.: Are glacials dry? Consequences for paleoclimatology and for greenhouse warming, J. Climate, 30, 6593–6609, https://doi.org/10.1175/JCLI-D-16-0854.1, 2017.

Schlesinger, W. H. and Jasechko, S.: Transpiration in the global water cycle, Agr. Forest Meteorol., 189, 115–117, https://doi.org/10.1016/j.agrformet.2014.01.011, 2014.

Sheng, E., Yu, K., Xu, H., Lan, J., Liu, B., and Che, S.: Late holocene Indian summer monsoon

https://doi.org/10.5194/cp-2021-55
Preprint. Discussion started: 3 June 2021

precipitation history at Lake Lugu, northwestern Yunnan Province, southwestern China, Palaeogeogra. Palaeocl., 438, 24–33, https://doi.org/10.1016/j.palaeo.2015.07.026, 2015.

Stabel, H.-H.: Calcite precipitation in Lake Constance: Chemical equilibrium, sedimentation, and nucleation by algae, Limnol. Oceanogr., 31, 1081–1093, https://doi.org/10.4319/lo.1986.31.5.1081, 1986.

Sun, S., Chen, H., Ju, W., Wang, G., Sun, G., Huang, J., Ma, H., Gao, C., Hua, W., and Yan, G.: On the coupling between precipitation and potential evapotranspiration: contributions to decadal drought anomalies in the Southwest China, Clim. Dynam., 48, 3779–3797, http://doi.org/10.1007/s00382-016-3302-5, 2017.

Sun, W., Zhang, E., Shulmeister, J., Bird, M. I., Chang, J., and Shen, J.: Abrupt changes in Indian summer monsoon strength during the last deglaciation and early Holocene based on stable isotope evidence from Lake Chenghai, southwest China, Quaternary Sci. Rev., 218, 1–9, https://doi.org/10.1016/j.quascirev.2019.06.006, 2019.

ter Braak, C. J. and Juggins, S.: Weighted averaging partial least squares regression (WA-PLS): an improved method for reconstructing environmental variables from species assemblages, Twelfth international diatom symposium, Renesse, The Netherlands, http://doi.org/10.1007/BF00028046, 1993.

Trenberth, K. E., Dai, A., Van Der Schrier, G., Jones, P. D., Barichivich, J., Briffa, K. R., and Sheffield, J.: Global warming and changes in drought, Nat. Clim. Change, 4, 17–22, https://doi.org/10.1038/nclimate2067, 2014.

Wang, G., Wang, Y., Wei, Z., He, W., Ma, X., and Zhang, T.: Reconstruction of temperature and precipitation spanning the past 28 kyr based on branched tetraether lipids from Qionghai Lake, southwestern China, Palaeogeogra. Palaeocl., 562, 110094, https://doi.org/10.1016/j.palaeo.2020.110094, 2020.

Wang, G., Wang, Y., Wei, Z., He, W., Ma, X., Sun, Z., Xu, L., Gong, J., Wang, Z., and Pan, Y.: Paleoclimate changes of the past 30 cal ka BP inferred from lipid biomarkers and geochemical records from Qionghai Lake, southwest China, J. Asian Earth Sci., 172, 346–358, https://doi.org/10.1016/j.jseaes.2018.09.019, 2019.

Wang, L., Yuan, X., Xie, Z., Wu, P., and Li, Y.: Increasing flash droughts over China during the recent global warming hiatus, Scientific Reports, 6, 30571, https://doi.org/10.1038/srep30571, 2016.

Wang, S. and Dou, H. (Eds.): The lake inventory of China, Science Press, Beijing, 1998.

Watras, C., Read, J., Holman, K., Liu, Z., Song, Y. Y., Watras, A., Morgan, S., and Stanley, E.: Decadal oscillation of lakes and aquifers in the upper Great Lakes region of North America: Hydroclimatic implications, Geophys. Res. Lett., 41, 456–462, https://doi.org/10.1002/2013GL058679, 2014.

Wei, G., Xie, L., Sun, Y., Lu, Y., and Liu, Y.: Major and trace elements of a peat core from Yunnan, Southwest China: implications for paleoclimatic proxies, J. Asian Earth Sci., 58, 64–77, https://doi.org/10.1016/j.jseaes.2012.06.021, 2012.

Whitmore, T. J., Brenner, M., Jiang, Z., Curtis, J. H., Moore, A., Engstrom, D. R., and Wu, Y.: Water quality and sediment geochemistry in lakes of Yunnan Province, southern China, Environ. Geol., 32, 45–55, https://doi.org/10.1007/s002540050192, 1997.

Wu, D., Zhou, A., Liu, J., Chen, X., Wei, H., Sun, H., Yu, J., Bloemendal, J., and Chen, F.: Changing intensity of human activity over the last 2,000 years recorded by the magnetic characteristics of sediments from Xingyun Lake, Yunnan, China, J. Paleolimnol., 53, 47–60, http://doi.org/10.1007/s10933-014-9806-2, 2015.

Wu, D., Chen, X., Lv, F., Brenner, M., Curtis, J., Zhou, A., Chen, J., Abbott, M., Yu, J., and Chen, F.: Decoupled early Holocene summer temperature and monsoon precipitation in southwest China, Quaternary Sci. Rev., 193, 54–67, https://doi.org/10.1016/j.quascirev.2018.05.038, 2018.

Xiao, J., Fan, J., Zhou, L., Zhai, D., Wen, R., and Qin, X.: A model for linking grain-size component to lake level status of a modern clastic lake, J. Asian Earth Sci., 69, 149–158, https://doi.org/10.1016/j.jseaes.2012.07.003, 2013.

Xiao, X., Haberle, S. G., Shen, J., Xue, B., Burrows, M., and Wang, S.: Postglacial fire history and interactions with vegetation and climate in southwestern Yunnan Province of China, Clim. Past, 13, 613–627, https://doi.org/10.5194/cp-13-613-2017, 2017.

Xiao, X., Haberle, S. G., Yang, X., Shen, J., Han, Y., and Wang, S.: New evidence on deglacial climatic variability from an alpine lacustrine record in northwestern Yunnan Province, southwestern China, Palaeogeogr. Palaeocl., 406, 9–21, https://doi.org/10.1016/j.palaeo.2014.04.008, 2014a.

Xiao, X., Haberle, S. G., Shen, J., Yang, X., Han, Y., Zhang, E., and Wang, S.: Latest Pleistocene and Holocene vegetation and climate history inferred from an alpine lacustrine record, northwestern Yunnan Province, southwestern China, Quaternary Sci. Rev., 86, 35–48, https://doi.org/10.1016/j.quascirev.2013.12.023, 2014b.

https://doi.org/10.5194/cp-2021-55
Preprint. Discussion started: 3 June 2021

Climate of the Past
Discussions

Xiao, X., Haberle, S. G., Li, Y., Liu, E., Shen, J., Zhang, E., Yin, J., and Wang, S.: Evidence of Holocene climatic change and human impact in northwestern Yunnan Province: High-resolution pollen and charcoal records from Chenghai Lake, southwestern China, Holocene, 28, 127–139, https://doi.org/10.1177/0959683617715692, 2018.

Xu, H., Lan, J., Zhang, G., and Zhou, X.: Arid Central Asia saw mid-Holocene drought, Geology, 47, 255–258, https://doi.org/10.1130/G45686.1, 2019.

Xu, Q., Li, Y., Yang, X., and Zheng, Z.: Quantitative relationship between pollen and vegetation in northern China, Sci. China Ser. D, 50, 582–599, http://doi.org/10.1007/s11430-007-2044-y, 2007.

Zhang, E., Chang, J., Shulmeister, J., Langdon, P., Sun, W., Cao, Y., Yang, X., and Shen, J.: Summer temperature fluctuations in Southwestern China during the end of the LGM and the last deglaciation, Earth Planet. Sc. Lett., 509, 78–87, https://doi.org/10.1016/j.epsl.2018.12.024, 2019a.

Zhang, E., Chang, J., Cao, Y., Sun, W., Shulmeister, J., Tang, H., Langdon, P. G., Yang, X., and Shen, J.: Holocene high-resolution quantitative summer temperature reconstruction based on subfossil chironomids from the southeast margin of the Qinghai-Tibetan Plateau, Quaternary Sci. Rev., 165, 1–12, https://doi.org/10.1016/j.quascirev.2017.04.008, 2017.

Zhang, L., Zhang, H., Chang, F., Duan, L., Hu, J., Li, T., Cai, M., and Zhang, Y.: Spatial variation characteristics of sediment size and its environmental indication significance in Lake Yilong, Yunnan Province, Quaternary Sci., 39, 1159–1170, http://doi.org/10.11928/j.issn.1001-7410.2019.05.08, 2019b. (in Chinese, with English abstract)

Zhang, Y.-K. and Schilling, K.: Effects of land cover on water table, soil moisture, evapotranspiration, and groundwater recharge: a field observation and analysis, J. Hydrol., 319, 328–338, https://doi.org/10.1016/j.jhydrol.2005.06.044, 2006.

Zhao, M., Li, H.-C., Liu, Z.-H., Mii, H.-S., Sun, H.-L., Shen, C.-C., and Kang, S.-C.: Changes in climate and vegetation of central Guizhou in southwest China since the last glacial reflected by stalagmite records from Yelang Cave, J. Asian Earth Sci., 114, 549–561, https://doi.org/10.1016/j.jseaes.2015.07.021, 2015.

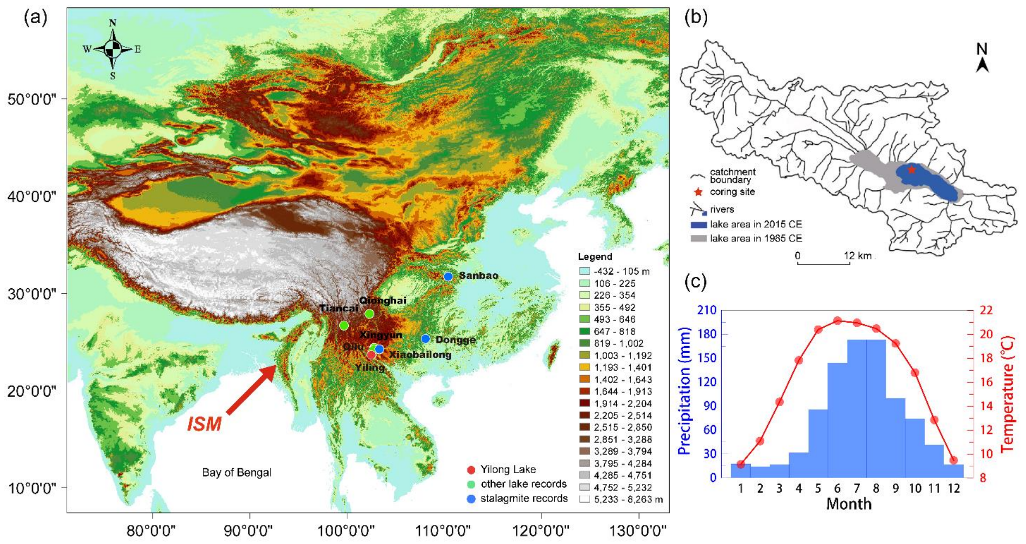

Figure 1. (a) Map showing the locations of Yilong Lake, other lake and stalagmite records; (b) catchment of the lake and the location of the core YLH; (c) average monthly temperature and precipitation during 1951–2017 CE (China Meteorological Data Service Centre, https://data.cma.cn/en).

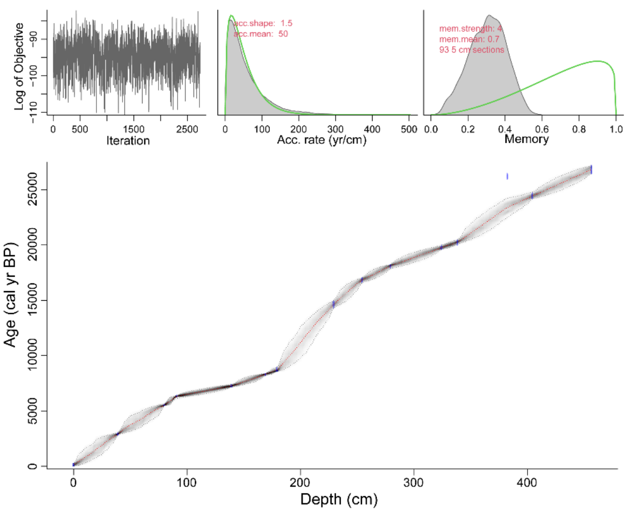

Figure 2. Age-depth model of core YLH.

https://doi.org/10.5194/cp-2021-55
Preprint. Discussion started: 3 June 2021

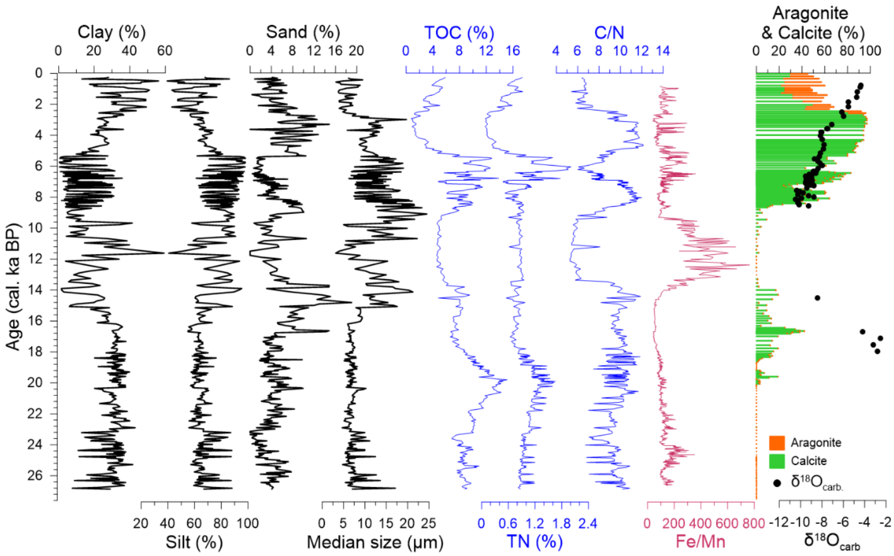

Figure 3. Down-core variations of grain-size components (clay, silt and sand), median grain size, TOC, TN, C/N ratio, Fe/Mn ratio, calcite and aragonite contents, and $\delta^{18}O_{carb}$.

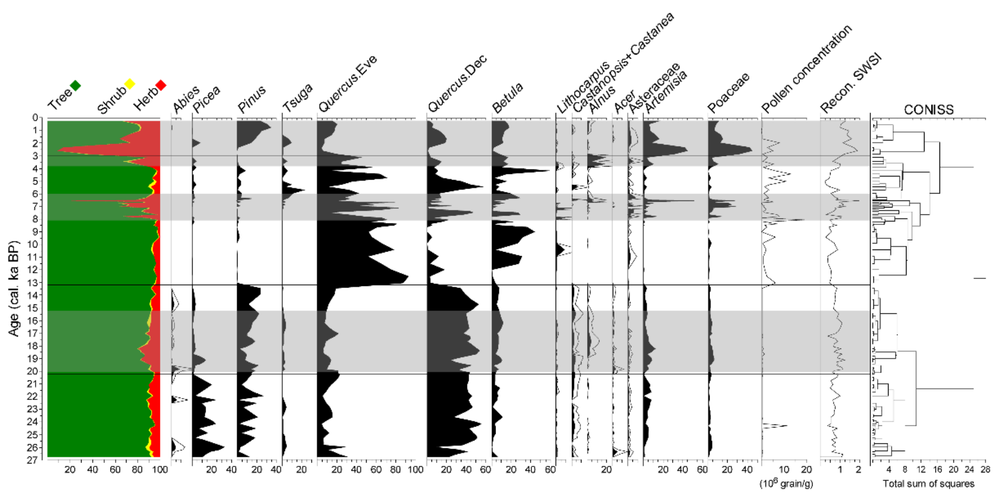

Figure 4. Pollen percentages of the main taxa (average percentages ≥ 5 %), pollen concentration and reconstructed SWSI. Pollen types with relatively low percentages have been magnified 3 times. Gray shadows mark relatively high SWSI.

https://doi.org/10.5194/cp-2021-55
Preprint. Discussion started: 3 June 2021

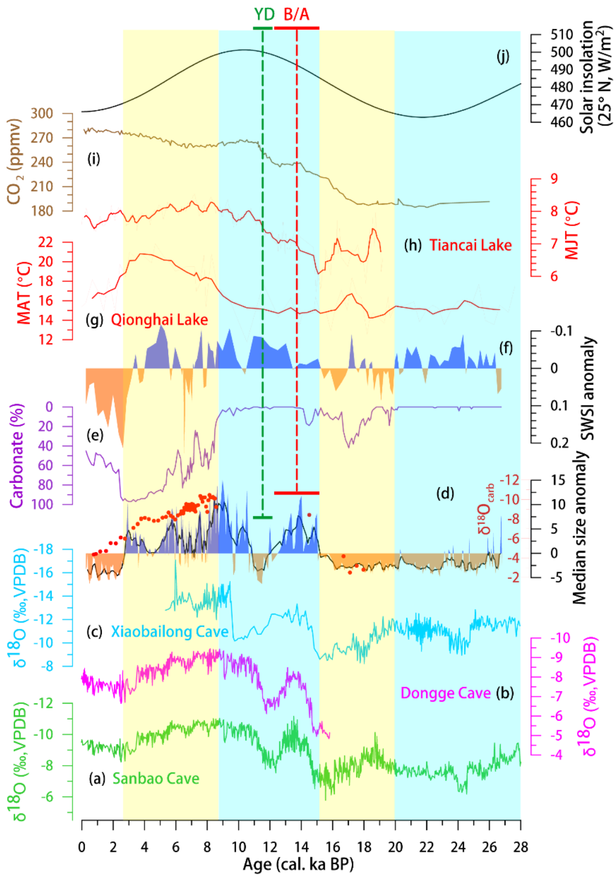

Figure 5. Stalagmite $\delta^{18}O$ records from Sanbao Cave (Cheng et al., 2016) (a), Dongge Cave (Dykoski et al., 2005) (b), and Xiaobailong Cave (Cai et al., 2015) (c); median size and $\delta^{18}O_{carb}$ (d), carbonate content (e), pollen-based reconstructed SWSI (f) from Yilong Lake (this study); (g) brGDGT-derived mean annual temperature (MAT) from Qionghai Lake (Wang et al., 2020); (h) chironomid-mean July temperature (MJT) from Tiancai Lake (Zhang et al., 2019a); (i) CO_2 concentration from Antarctic ice core record (Ahn et al., 2004); (j) Summer insolation curve for 25° N.

661 **Table 1.** AMS ^{14}C results of the sediment core YLH.

Lab ID	Depth (cm)	Materials	IRMS $\delta^{13}C$ (‰)	Conventional Radiocarbon Age (yr BP)	Calibrated Age (2 σ, cal. yr BP)
Beta-468347	1	Sediment-TOC	24.6	-30 +/- 30	100.37 +/- 0.37 pMC
Beta-492284	40	Charcoal and plant remains	-21.5	2820 +/- 30	2848–3004
Beta-492285	80	Charcoal and plant remains	-20	4820 +/- 30	5477–5539
Beta-468348	91	Sediment-TOC	-27.3	5560 +/- 30	6297–6398
Beta-492286	140	Charcoal and plant remains	-18.7	6330 +/- 30	7237–7318
Beta-468349	170	Charcoal and plant remains	-21.5	7510 +/- 30	8289–8386
Beta-492287	180	Charcoal and plant remains	-28.7	7860 +/- 30	8585–8771
Beta-492288	230	Charcoal and plant remains	-13.1	12460 +/- 40	14322–14745
Beta-468350	255	Sediment-TOC	-17.6	13880 +/- 40	16678–17025
Beta-492289	280	Sediment-TOC	-18.8	14800 +/- 40	17986–18242
Beta-468351	325	Sediment-TOC	-19.9	16400 +/- 50	19582–19923
Beta-541605	338	Plant remains	-27	16730 +/- 50	20058–20408
Beta-468352	383	Sediment-TOC	-19.3	21980 +/- 70	25973–26393
Beta-537522	404	Charcoal	-25.1	20320 +/- 70	24183–24631
Beta-468353	457	Plant remains	-17.8	22560 +/- 80	26829–27171

662